6-dialkylamino-2-naphthylethylidene derivatives as positron emission tomography imaging probes for beta-amyloid plaques in Alzheimer's disease. J Neurosci 2001; 21: RC189.

Arriagada PV, Growdon JH, Hedley-Whyte ET, Hyman BT. Neurofibrillary tangles but not senile plaques parallel duration and severity of Alzheimer's disease. Neurology 1992; 42 (3 Pt 1): 631–9.

Barghorn S, Davies P, Mandelkow E. Tau paired helical filaments from Alzheimer's disease brain and assembled in vitro are based on beta-structure in the core domain. Biochemistry 2004; 43: 1694–703.

Blennow K, Hampel H. CSF markers for incipient Alzheimer's disease. Lancet Neurol 2003; 2: 605–13.

Cairns NJ, Ikonomovic MD, Benzinger T, Storandt M, Fagan AM, Shah A, et al. Absence of Pittsburgh compound B detection of cerebralamyloid beta in a patient with clinical, cognitive, and cerebrospinal fluidmarkers of Alzheimer disease. Arch Neurol 2009; 66: 1557–62.

Choi SR, Golding G, Zhuang Z, Zhang W, Lim N, Hefti F, et al. Preclinical properties of 18F-AV-45: a PET agent for Abeta plaques in the brain. J Nucl Med 2009; 50: 1887–94.

Delaere P, Duyckaerts C, Brion JP, Poulain V, Hauw JJ. Tau, paired helical filaments and amyloid in the neocortex: a morphometric study of 15 cases with graded intellectual status in aging and senile dementia of Alzheimer type. Acta neuropathologica 1989; 77: 645–53.

Delaere P, Duyckaerts C, Masters C, Beyreuther K, Piette F, Hauw JJ. Large amounts of neocortical beta A4 deposits without neuritic plaques nor tangles in a psychometrically assessed, non-demented person. Neurosci Lett 1990; 116: 87–93.

Dickson DW. Neuropathological diagnosis of Alzheimer's disease: a perspective from longitudinal clinicopathological studies. Neurobiology of aging 1997; 18 (Suppl 4): S21–6.

Dishino DD, Welch MJ, Kilbourn MR, Raichle ME. Relationship between lipophilicity and brain extraction of C-11-labeled radiopharmaceuticals. J Nucl Med 1983; 24: 1030–8.

Duyckaerts C, Brion JP, Hauw JJ, Flament-Durand J. Quantitative assessment of the density of neurofibrillary tangles and senile plaques in senile dementia of the Alzheimer type. Comparison of immunocytochemistry with a specific antibody and Bodian's protargol method. Acta neuropathologica 1987; 73: 167–70.

Duyckaerts C, Delaere P, Hauw JJ, Abbamondi-Pinto AL, Sorbi S, Allen I, et al. Rating of the lesions in senile dementia of the Alzheimer type: concordance between laboratories. A European multicenter study under the auspices of EURAGE. J Neurol Sci 1990; 97: 295–323.

Ferreira ST, Vieira MN, De Felice FG. Soluble protein oligomers as emerging toxins in Alzheimer's and other amyloid diseases. IUBMB Life 2007; 59: 332–45.

Fodero-Tavoletti MT, Rowe CC, McLean CA, Leone L, Li QX, Masters CL, et al. Characterization of PiB binding to white matter in Alzheimer disease and other dementias. J Nucl Med 2009; 50: 198–204.

Fodero-Tavoletti MT, Smith DP, McLean CA, Adlard PA, Barnham KJ, Foster LE, et al. In vitro characterization of Pittsburgh compound-B binding to Lewy bodies. J Neurosci 2007; 27: 10365–71.

Ganzer S, Arlt S, Schoder V, Buhmann C, Mandelkow EM, Finckh U, et al. CSF-tau, CSF-Abeta1-42, ApoE-genotype and clinical parameters in the diagnosis of Alzheimer's disease: combination of CSF-tau and MMSE yields highest sensitivity and specificity. J Neural Transm 2003; 110: 1149–60.

Gozes I, Stewart A, Morimoto B, Fox A, Sutherland K, Schmeche D. Addressing Alzheimer's disease tangles: from NAP to AL-108. Curr Alzheimer Res 2009; 6: 455–60.

Hampel H, Blennow K, Shaw LM, Hoessler YC, Zetterberg H, Trojanowski JQ. Total and phosphorylated tau protein as biological markers of Alzheimer's disease. Exp Gerontol 2009a; 45: 30–40.

Hampel H, Ewers M, Burger K, Annas P, Mortberg A, Bogstedt A, et al. Lithium trial in Alzheimer's disease: a randomized, single-blind, placebo-controlled, multicenter 10-week study. J Clin Psychiatry 2009b; 70: 922–31.

Ho GJ, Gregory EJ, Smirnova IV, Zoubine MN, Festoff BW. Cross-linking of beta-amyloid protein precursor catalyzed by tissue transglutaminase. FEBS Lett 1994; 349: 151–4.

Holcomb LA, Gordon MN, Jantzen P, Hsiao K, Duff K, Morgan D. Behavioral changes in transgenic mice expressing both amyloid precursor protein and presenilin-1 mutations: lack of association with amyloid deposits. Behav Genet 1999; 29: 177–85.

Ikonomovic MD, Klunk WE, Abrahamson EE, Mathis CA, Price JC, Tsopelas ND, et al. Post-mortem correlates of in vivo PiB-PET amyloid imaging in a typical case of Alzheimer's disease. Brain 2008; 131 (Pt 6): 1630–45.

Jack CR Jr, Knopman DS, Jagust WJ, Shaw LM, Aisen PS, Weiner MW, et al. Hypothetical model of dynamic biomarkers of the Alzheimer's pathological cascade. Lancet Neurol 2010; 9: 119–28.

Katzman R, Terry R, DeTeresa R, Brown T, Davies P, Fuld P, et al. Clinical, pathological, and neurochemical changes in dementia: a subgroup with preserved mental status and numerous neocortical plaques. Ann Neurol 1988; 23: 138–44.

Kepe V, Huang SC, Small GW, Satyamurthy N, Barrio JR. Visualizing pathology deposits in the living brain of patients with Alzheimer's disease. Methods Enzymol 2006; 412: 144–60.

Klunk WE, Engler H, Nordberg A, Wang Y, Blomqvist G, Holt DP, et al. Imaging brain amyloid in Alzheimer's disease with Pittsburgh Compound-B. Ann Neurol 2004; 55: 306–19.

Klunk WE, Lopresti BJ, Ikonomovic MD, Lefterov IM, Koldamova RP, Abrahamson EE, et al. Binding of the positron emission tomography tracer Pittsburgh compound-B reflects the amount of amyloid-beta in Alzheimer's disease brain but not in transgenic mouse brain. J Neurosci 2005; 25: 10598–606.

Lambert MP, Viola KL, Chromy BA, Chang L, Morgan TE, Yu J, et al. Vaccination with soluble Abeta oligomers generates toxicity-neutralizing antibodies. J Neurochem 2001; 79: 595–605.

Laruelle M, Slifstein M, Huang Y. Relationships between radiotracer properties and image quality in molecular imaging of the brain with positron emission tomography. Mol Imaging Biol 2003; 5: 363–75.

Lee VM, Goedert M, Trojanowski JQ. Neurodegenerative tauopathies. Annu Rev Neurosci 2001; 24: 1121–59.

LeVine H 3rd. Quantification of beta-sheet amyloid fibril structures with thioflavin T. Methods Enzymol 1999; 309: 274–84.

Maeda J, Ji B, Irie T, Tomiyama T, Maruyama M, Okauchi T, et al. Longitudinal, quantitative assessment of amyloid, neuroinflammation, and anti-amyloid treatment in a living mouse model of Alzheimer's disease enabled by positron emission tomography. J Neurosci 2007; 27: 10957–68.

Maezawa I, Hong HS, Liu R, Wu CY, Cheng RH, Kung MP, et al. Congo red and thioflavin-T analogs detect Abeta oligomers. J Neurochem 2008; 104: 457–68.

McLean CA, Cherny RA, Fraser FW, Fuller SJ, Smith MJ, Beyreuther K, et al. Soluble pool of Abeta amyloid as a determinant of severity of neurodegeneration in Alzheimer's disease. Annals Neurol 1999; 46: 860–6.

Ng S, Villemagne VL, Berlangieri S, Lee ST, Cherk M, Gong SJ, et al. Visual assessment versus quantitative assessment of 11C-PIB PET and 18F-FDG PET for detection of Alzheimer's disease. J Nucl Med 2007; 48: 547–52.

Nordberg A. PET imaging of amyloid in Alzheimer's disease. Lancet Neurol 2004; 3: 519–27.

Okamura N, Suemoto T, Furumoto S, Suzuki M, Shimadzu H, Akatsu H, et al. Quinoline and benzimidazole derivatives: candidate probes for in vivo imaging of tau pathology in Alzheimer's disease. J Neurosci 2005; 25: 10857–62.

Perez M, Valpuesta JM, Medina M, Montejo de Garcini E, Avila J. Polymerization of tau into filaments in the presence of heparin: the minimal sequence required for tau-tau interaction. J Neurochem 1996; 67: 1183–90.

Pike VW. PET radiotracers: crossing the blood-brain barrier and surviving metabolism. Trends Pharmacol Sci 2009; 30: 431–40.

Pike KE, Savage G, Villemagne VL, Ng S, Moss SA, Maruff P, et al. Beta-amyloid imaging and memory in non-demented individuals: evidence for preclinical Alzheimer's disease. Brain 2007; 130 (Pt 11): 2837–44.

Rowe CC, Ackerman U, Browne W, Mulligan R, Pike KL, O'Keefe G, et al. Imaging of amyloid beta in Alzheimer's disease with 18F-BAY94-9172, a novel PET tracer: proof of mechanism. Lancet Neurol 2008; 7: 129–35.

Rowe CC, Ng S, Ackermann U, Gong SJ, Pike K, Savage G, et al. Imaging beta-amyloid burden in aging and dementia. Neurology 2007; 68: 1718–25.

Shoghi-Jadid K, Small GW, Agdeppa ED, Kepe V, Ercoli LM, Siddarth P, et al. Localization of neurofibrillary tangles and beta-amyloid plaques in the brains of living patients with Alzheimer disease. Am J Geriatr Psychiatry 2002; 10: 24–35.

van der Zee J, Sleegers K, Van Broeckhoven C. Invited article: the Alzheimer disease-frontotemporal lobar degeneration spectrum. Neurology 2008; 71: 1191–7.

Van Dort ME, Jung YW, Sherman PS, Kilbourn MR, Wieland DM. Fluorine for hydroxy substitution in biogenic amines: asymmetric synthesis and biological evaluation of fluorine-18-labeled beta-fluorophenylalkylamines as model systems. J Med Chem 1995; 38: 810–5.

von Bergen M, Barghorn S, Jeganathan S, Mandelkow EM, Mandelkow E. Spectroscopic approaches to the conformation of tau protein in solution and in paired helical filaments. Neurodegener Dis 2006; 3: 197–206.

Walsh DM, Klyubin I, Fadeeva JV, Cullen WK, Anwyl R, Wolfe MS, et al. Naturally secreted oligomers of amyloid beta protein potently inhibit hippocampal long-term potentiation in vivo. Nature 2002; 416: 535–9.

Wenk GL. Neuropathologic changes in Alzheimer's disease. J Clin Psychiatry 2003; 64 (Suppl 9): 7–10.

Wischik C, Staff R. Challenges in the conduct of disease-modifying trials in Alzheimer's disease: practical experience from a phase 2 trial of Tau-aggregation inhibitor therapy. J Nutr Health Aging 2009; 13: 367–9.

Wisniewski HM, Bancher C, Barcikowska M, Wen GY, Currie J. Spectrum of morphological appearance of amyloid deposits in Alzheimer's disease. Acta Neuropathol 1989; 78: 337–47.

Eur J Nucl Med Mol Imaging (2010) 37:934–941
DOI 10.1007/s00259-009-1314-7

ORIGINAL ARTICLE

In vivo detection of prion amyloid plaques using [^{11}C]BF-227 PET

Nobuyuki Okamura · Yusei Shiga · Shozo Furumoto · Manabu Tashiro · Yoshio Tsuboi · Katsutoshi Furukawa · Kazuhiko Yanai · Ren Iwata · Hiroyuki Arai · Yukitsuka Kudo · Yasuhito Itoyama · Katsumi Doh-ura

Received: 7 August 2009 / Accepted: 21 October 2009 / Published online: 17 December 2009

Abstract
Purpose In vivo detection of pathological prion protein (PrP) in the brain is potentially useful for the diagnosis of transmissible spongiform encephalopathies (TSEs). However, there are no non-invasive ante-mortem means for detection of pathological PrP deposition in the brain. The purpose of this study is to evaluate the amyloid imaging tracer BF-227 with positron emission tomography (PET) for the non-invasive detection of PrP amyloid in the brain.
Methods The binding ability of BF-227 to PrP amyloid was investigated using autoradiography and fluorescence microscopy. Five patients with TSEs, including three patients with Gerstmann-Sträussler-Scheinker disease (GSS) and two patients with sporadic Creutzfeldt-Jakob disease (CJD), underwent [^{11}C]BF-227 PET scans. Results were compared with data from 10 normal controls and 17 patients with Alzheimer's disease (AD). The regional to pons standardized uptake value ratio was calculated as an index of BF-227 retention.
Results Binding of BF-227 to PrP plaques was confirmed using brain samples from autopsy-confirmed GSS cases. In clinical PET study, significantly higher retention of BF-227 was detected in the cerebellum, thalamus and lateral temporal cortex of GSS patients compared to that in the corresponding tissues of normal controls. GSS patients also showed higher retention of BF-227 in the cerebellum, thalamus and medial temporal cortex compared to AD patients. In contrast, the two CJD patients showed no obvious retention of BF-227 in the brain.
Conclusion Although [^{11}C]BF-227 is a non-specific imaging marker of cerebral amyloidosis, it is useful for in vivo detection of PrP plaques in the human brain in GSS, based on the regional distribution of the tracer. PET amyloid imaging might provide a means for both early diagnosis and non-invasive disease monitoring of certain forms of TSEs.

N. Okamura · S. Furumoto · K. Yanai
Department of Pharmacology,
Tohoku University School of Medicine,
Sendai, Japan

Y. Shiga · Y. Itoyama
Department of Neurology,
Tohoku University School of Medicine,
Sendai, Japan

S. Furumoto · R. Iwata
Division of Radiopharmaceutical Chemistry,
Cyclotron and Radioisotope Center, Tohoku University,
Sendai, Japan

M. Tashiro
Division of Cyclotron Nuclear Medicine,
Cyclotron and Radioisotope Center, Tohoku University,
Sendai, Japan

Y. Tsuboi
Department of Neurology,
Fukuoka University School of Medicine,
Fukuoka, Japan

K. Furukawa · H. Arai
Department of Geriatrics and Gerontology,
Division of Brain Sciences, Institute of Development,
Aging, and Cancer, Tohoku University,
Sendai, Japan

Y. Kudo
Innovation of New Biomedical Engineering Center,
Tohoku University,
Sendai, Japan

K. Doh-ura (✉)
Department of Prion Research,
Tohoku University School of Medicine,
2-1 Seiryo-machi, Aoba-ku, Sendai 980-8575, Japan
e-mail: doh-ura@mail.tains.tohoku.ac.jp

Keywords Prion · PET · Amyloid · Creutzfeldt-Jakob disease

Introduction

Transmissible spongiform encephalopathies (TSEs), also known as prion diseases, are a group of fatal neurodegenerative disorders, including Creutzfeldt-Jakob disease (CJD), Gerstmann-Sträussler-Scheinker disease (GSS) and kuru [1–3]. TSEs are characterized by progressive deposition of abnormal prion protein (PrP) in the brain. CJD is the most common type of human TSE and is classified into sporadic, genetic and infectious forms according to the aetiology of illness. GSS is a familial neurodegenerative disorder associated with mutations of the PrP gene and is clinically recognized by cerebellar ataxia combined with postural abnormalities and cognitive decline [1–3]. Two major types of abnormal PrP deposition, synaptic and plaque types, have been described in the brain of people with TSEs [1]. The synaptic type of PrP deposition, which does not have tinctorial properties of amyloid in tissue sections, is most commonly observed in sporadic CJD, whereas the plaque type, which frequently forms congophilic amyloid plaques, is a hallmark of such TSEs as GSS, variant CJD (vCJD) and iatrogenic dura CJD with plaques [1, 4]. Abnormal PrP deposition in the brain is suggested to start before the occurrence of clinical symptoms [5–7]. Thus, preclinical diagnosis and, when available, early disease-specific therapeutic interventions, can be beneficial for people predisposed to or affected by TSEs.

Several positron emission tomography (PET) imaging agents have been recently developed and used for in vivo detection of brain amyloid-β (Aβ) plaques in patients with Alzheimer's disease (AD) [8–12]. Most of these β-sheet binding agents show high binding affinity to PrP amyloid because PrP aggregates in TSEs form β-pleated sheet structures and share a common secondary structure with Aβ deposits in AD brains [13–16]. Therefore, these agents would be useful for the in vivo detection of PrP amyloid in the brain. Two clinical PET studies were performed using [^{18}F]FDDNP and/or [^{11}C]PIB in sporadic and familial CJD patients [17, 18]. The results indicated moderate retention of FDDNP and no obvious retention of PIB in the brain [17, 18]. Therefore, agents that can sensitively detect abnormal PrP deposits should be further explored for the diagnosis of TSEs. We have demonstrated in vitro and in vivo binding of benzoxazole derivatives to both Aβ and PrP amyloids [19, 20]. One of these derivatives, BF-227, was used for a clinical PET study where it successfully visualized amyloid deposits in the brain of AD patients in vivo [12, 21]. Therefore, [^{11}C]BF-227 appears to be a promising candidate for PET imaging of PrP deposits. The purpose of this study was to evaluate the clinical utility of [^{11}C]BF-227 PET for the non-invasive detection of abnormal PrP deposits in patients with TSEs.

Methods

Preparation of compounds

BF-227 and its 2-tosyloxyethoxy and *N*-desmethylated derivatives were custom synthesized by Tanabe R&D Service Co. (Osaka, Japan). [^{18}F]BF-227 was synthesized for autoradiography of brain sections, as described previously [22]. For the clinical studies, [^{11}C]BF-227 was synthesized as described previously [12]. Radiochemical yields were greater than 50% based on [^{11}C]methyl triflate, and specific radioactivities were 119–138 GBq/μmol at the end of synthesis. Radiochemical purities were greater than 95%.

Histopathological staining and in vitro autoradiography

Autopsy-diagnosed brain samples from two GSS cases with PrP plaque deposition and two sporadic CJD cases with synaptic PrP deposition were provided by Dr. Toru Iwaki of the Department of Neuropathology, Kyushu University, Japan. The brain sample from an 81-year-old man with autopsy-confirmed physiological aging was obtained from Tohoku University Hospital. The two GSS cases had a proline-to-leucine mutation at codon 102 and methionine homozygosity at codon 129 of the PrP gene, and the two sporadic CJD cases had no mutations and methionine homozygosity at codon 129; they showed type 1 abnormal PrP in immunoblotting of the brain tissues. All of the brain samples were treated with 98% formic acid for 1 h before paraffin embedding to eliminate prion infectivity. Sections from paraffin-embedded blocks of the cerebellum or frontal cortex were then dewaxed in xylene and ethanol. For staining with BF-227, tissue sections were immersed in 100 μM BF-227 solution containing 50% ethanol for 10 min. They were then dipped briefly into water and rinsed in phosphate-buffered saline for 10 min before coverslipping with FluorSave Reagent (Calbiochem, La Jolla, CA, USA). Subsequently, they were examined using an Eclipse E800 microscope (Nikon, Tokyo, Japan) equipped with a V-2A filter set (excitation, 380–420 nm; dichroic mirror, 430 nm; Longpass filter, 450 nm). For autoradiography, the section was incubated with 1.0 MBq/ml of [^{18}F]BF-227 at room temperature for 10 min and then washed briefly with water and 50% ethanol. After drying, the labelled section was exposed to a BAS-III imaging plate (Fuji Film, Tokyo, Japan) overnight. Autoradiographic images were obtained using a BAS-5000 phosphor imaging instrument (Fuji Film, Tokyo, Japan). Neighbouring sec-

tions were immunostained using 3F4 anti-PrP monoclonal antibody (Covance, Princeton, NJ, USA) as described previously [13, 20].

Subjects and patients in the clinical PET study

Five TSE patients, including two sporadic CJD patients [63-year-old woman (CJD1) and 58-year-old man (CJD2)] and three GSS patients [69-year-old woman (GSS1), 61-year-old man (GSS2) and 30-year-old woman (GSS3)], underwent PET scans with [^{11}C]BF-227 (Table 1). For comparison, [^{11}C]BF-227 PET studies were also performed in 17 AD patients [mean age ± standard deviation (SD)= 72.6±6.7; mean Mini-Mental State Examination score ± SD=19.8±4.0] and 10 aged normal controls (mean age ± SD=67.2±2.5). Some of these AD and normal subjects were included in our previous report [12].

CJD1's health was unremarkable until the manifestation of depressive symptoms at the age of 62 years. The patient then developed subacutely progressive dementia, motor disturbances and myoclonus. CJD2 showed subacutely progressive dementia and gait disturbance and then developed psychotic symptoms, dysarthria and myoclonus. Both CJD patients had no mutations and showed methionine homozygosity at codon 129 of the PrP gene. PET studies in CJD1 and CJD2 were performed when they reached grade 4 of the modified Rankin scale at 3 and 4 months after onset of symptoms, respectively. Both patients showed periodic synchronous discharges in electroencephalograms and hyperintensity in the caudate, putamen and cerebral cortex on diffusion-weighted magnetic resonance (MR) images. Diagnosis of probable CJD was made according to the WHO criteria [23].

Each GSS patient was from a different pedigree and had a family history of the same disease, carrying a proline-to-leucine mutation at codon 102 and methionine homozygosity at codon 129 of the PrP gene. GSS1 and GSS2, having a 9- and 20-month clinical duration from the onset, respectively, showed signs of moderate cerebellar ataxia, such as gait disturbance and slurred speech; however, they could walk unassisted and had slight or no cognitive impairment. GSS1 and GSS2 scored 22 and 26 points, respectively, on the Mini-Mental State Examination. GSS3, having a 27-month clinical duration, showed severe gait disturbance and slurred speech and was unable to walk unassisted; however, she had no cognitive impairment (30 points on the Mini-Mental State Examination) at the time of this study.

AD diagnosis was made according to the National Institute of Neurological and Communicative Diseases and Stroke-Alzheimer's Disease and Related Disorders Association (NINCDS-ADRDA) criteria [24]. CJD, GSS and AD patients were recruited from Miyagi National Hospital, Fukuoka University Hospital, Kagoshima University Hospital and Tohoku University Hospital. Normal controls were recruited from volunteers with no cognitive impairment or cerebrovascular lesions on MR images and who were not taking any centrally acting medications. No significant difference in age distribution was apparent between the groups. This study was approved by the Ethics Committee on clinical investigations of Tohoku University School of Medicine and performed in accordance with the Declaration of Helsinki. Written informed consent was obtained after complete description of the study to the patients and subjects.

Image acquisition protocols

PET scans were performed using a SET-2400W (Shimadzu Inc., Kyoto, Japan). After intravenous injection of 211–366 MBq (5.7–9.9 mCi) of [^{11}C]BF-227, dynamic PET images were obtained for 60 min with the subjects' eyes closed. Arterial blood sampling in the TSE patients was not

Table 1 Regional to pons standardized uptake value ratio (SUVRp) values in aged normal controls (Control), Alzheimer's disease patients (AD), Creutzfeldt-Jakob disease patients (CJD) and Gerstmann-Sträussler-Scheinker disease patients (GSS)

	Control (n=10) Mean ± SD	AD (n=17) Mean ± SD	CJD1	CJD2	GSS (n=3) Mean ± SD	GSS1	GSS2	GSS3
Frontal	0.60±0.03	0.64±0.04	0.57	0.61	0.67±0.08	0.74	0.69	0.57
Lateral temporal	0.59±0.03	0.69±0.04*	0.63	0.62	0.67±0.05*	0.71	0.68	0.61
Parietal	0.62±0.02	0.69±0.04*	0.62	0.62	0.67±0.06	0.72	0.68	0.61
Occipital	0.62±0.04	0.65±0.05	0.62	0.69	0.67±0.07	0.74	0.67	0.60
Medial temporal	0.64±0.04	0.62±0.03	0.57	0.65	0.67±0.02**	0.66	0.70	0.67
Striatum	0.71±0.04	0.75±0.04*	0.69	0.72	0.76±0.04	0.80	0.77	0.72
Thalamus	1.00±0.04	1.01±0.04	0.97	1.04	1.08±0.00*, **	1.08	1.07	1.08
Cerebellum	0.58±0.01	0.57±0.02	0.58	0.59	0.62±0.01*, **	0.61	0.63	0.61

*p<0.05 compared to aged normal group

**p < 0.05 compared to AD group

performed because the Committee on Clinical Investigation at Tohoku University School of Medicine did not approve blood sampling during the PET scan, from the standpoint of infection risk management. T_1-weighted MR images were obtained using a Signa 1.5-T machine (General Electric Inc., Milwaukee, WI, USA).

Image analysis

Standardized uptake value (SUV) images of [^{11}C]BF-227 were obtained by normalizing tissue concentration by injected dose and body weight. Average summations of SUV images were created from early frames (0–30 min post-injection) and late frames (40–60 min post-injection) of dynamic PET images. Early frame images were created for co-registration with individual MR images, and late frame images were used for calculation of SUV. Individual MR images were anatomically co-registered with the early frame PET images using statistical parametric mapping software (SPM2, Welcome Department of Imaging Neuroscience, London, UK) [25]. Spatial normalization was performed using an MR T_1 template of SPM2 to transfer PET images into a standard stereotactic space. Regions of interest (ROIs) were placed on a spatially normalized MR image, as described previously [12]. ROI information was then copied onto delayed PET SUV images, and regional SUV images at 40–60 min post-injection were sampled using Dr.View/LINUX software (AJS, Tokyo, Japan). Deposition of PrP plaques is reportedly frequent in the cerebellum but scarce in the pons of GSS brain [26]. Furthermore, BF-227 retention in the pons does not differ between AD patients and normal controls. Therefore, we used the pons as a reference region and calculated the regional to pons SUV ratio (SUVRp) as an index of BF-227 retention.

Statistical analysis

For statistical comparison in each group, we applied one-way analysis of variance, followed by the Bonferroni-Dunn post hoc test. Statistical comparison of age distribution was performed using the Kruskal-Wallis test, followed by Dunn's multiple comparison test. Statistical significance for each analysis was defined as $p<0.05$.

Results

Autoradiography examination indicated binding of a tracer dose of BF-227 to PrP plaque deposits. BF-227 retention was present in brain sections from GSS cases with PrP plaque deposition but not from normal control cases and sporadic CJD cases with synaptic PrP deposition (Fig. 1a–c). The regional distribution of [^{18}F]BF-227 in the autoradiograms co-localized with the immunostained PrP plaques in the cerebellar cortex of GSS cases (Fig. 1d–e). BF-227 binding to PrP plaques was additionally examined using a microscope, because BF-227 is a fluorescent compound. Core regions of the PrP plaques were intensely stained with BF-227 (Fig. 2, arrows), indicating that BF-227 preferentially binds to the fibril-rich core of PrP amyloid plaques.

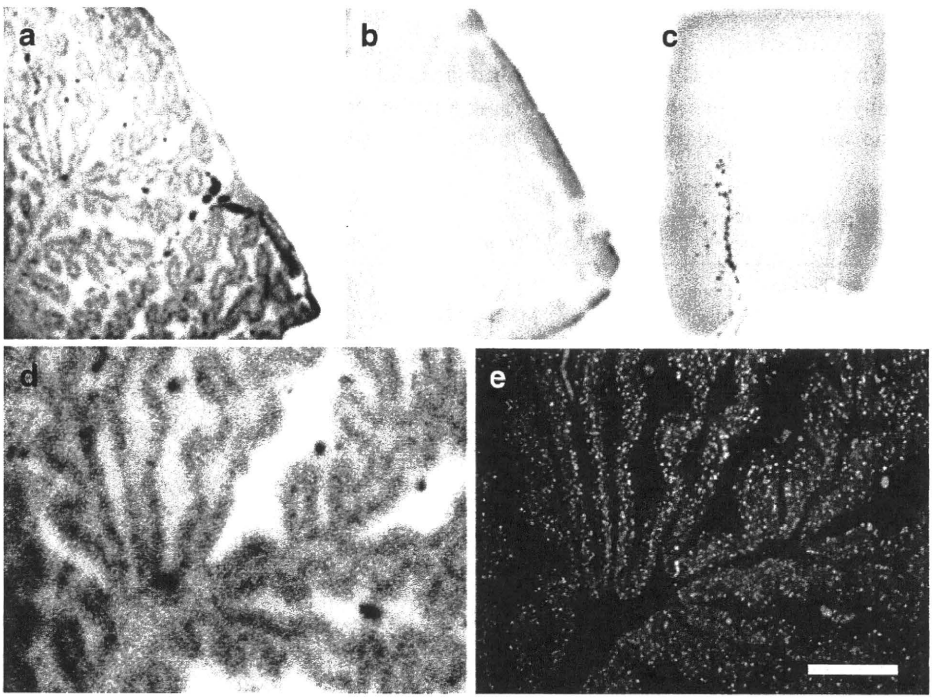

Fig. 1 [^{18}F]BF-227 autoradiograms of a cerebellar section from a Gerstmann-Sträussler-Scheinker (GSS) case (**a**), a cerebellar section from a physiological aging case (**b**) and a frontal cortex section from a sporadic Creutzfeldt-Jakob disease (CJD) case (**c**) are shown, together with a magnified view of **a** (**d**) and prion protein (PrP) immunostaining of the same field as **d** (**e**). BF-227 retention was present in the brain section from a GSS case with PrP plaque deposition, but not from a normal control case and sporadic CJD case with synaptic PrP deposition. *Bar*=200 μm

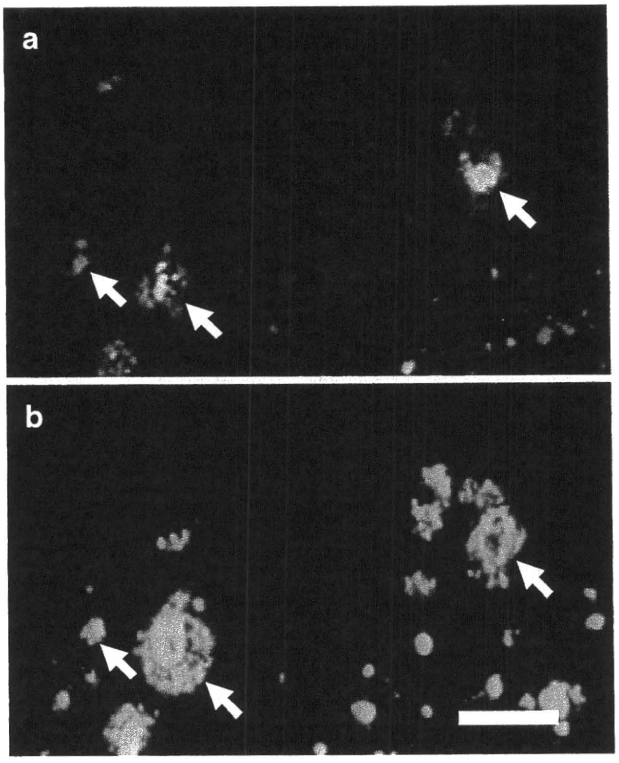

Fig. 2 Microscopic images of BF-227 staining (**a**) and PrP immunostaining (**b**) of the cerebellar cortex of a GSS case. *Arrows* indicate PrP amyloid plaques. The core regions of PrP plaques were intensely stained with BF-227. *Bar*=50 μm

Figure 3 shows the average summations of SUVRp images in an aged normal subject (64-year-old man), a sporadic CJD patient (CJD1, 63-year-old woman), a GSS patient (GSS2, 61-year-old man) and an AD patient (62-year-old woman). As reported previously, non-specific retention of [^{11}C]BF-227 was observed in the brain stem and white matter of all subjects [12]. The GSS patient showed obvious retention of [^{11}C]BF-227 in the cerebellum, and lateral and medial temporal cortices. The three GSS patients showed significantly higher SUVRp in the lateral temporal cortex, thalamus and cerebellum (Table 1, Fig. 4) when compared to aged normal controls. Furthermore, when compared to the AD group, the GSS group showed significant elevation of SUVRp in the medial temporal cortex, thalamus and cerebellum. Although two GSS patients (GSS1 and GSS2) showed retention of BF-227 in most brain regions, the youngest GSS patient (GSS3) showed BF-227 retention only in the cerebellum, thalamus and medial temporal cortex, but not in the neocortex (Table 1, Fig. 4). Furthermore, two sporadic CJD patients showed no obvious BF-227 retention in any of the brain regions examined (Table 1, Fig. 4). As previously described [12, 21], AD patients showed [^{11}C]BF-227 retention in the neocortex; however, the cerebellum and medial temporal cortex were relatively spared (Table 1).

Autopsy examination of the brain of one GSS patient (GSS1) confirmed both the presence of abundant PrP amyloid plaques in the neocortex, cerebellum, basal ganglia, thalamus, entorhinal cortex and hippocampus and the absence of Aβ amyloid plaques or other structures of misfolded protein deposition such as Lewy bodies and neurofibrillary tangles. When compared to controls, the highest SUVRp percentage difference was found in the neocortex, especially in the frontal cortex (22%), followed by the striatum (12%), thalamus (9%), cerebellum (6%) and medial temporal cortex (3%) in this case. This finding was consistent with the autopsy result showing higher density of PrP amyloid plaques in the neocortex and basal ganglia than in the cerebellum, thalamus and hippocampus. Details of clinicopathological features of this case will be published elsewhere.

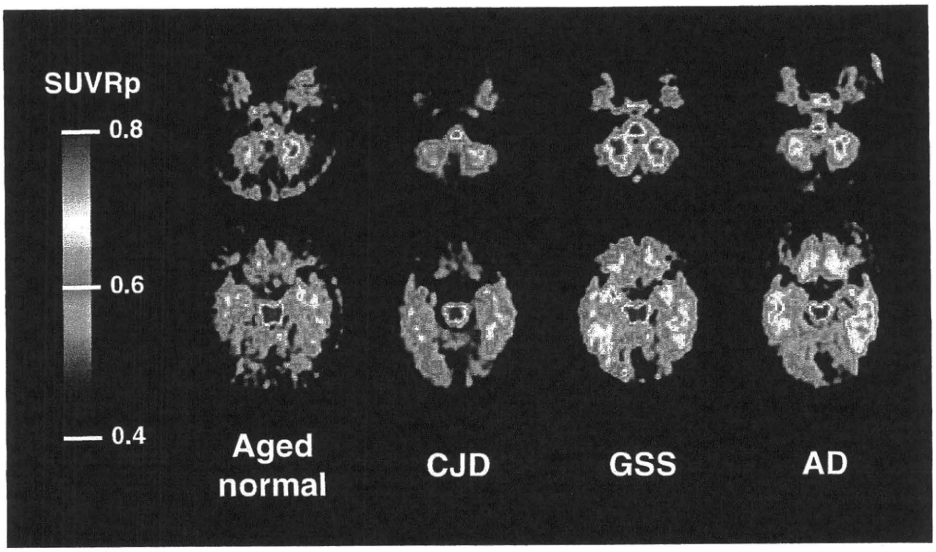

Fig. 3 Mean regional to pons standardized uptake value ratio (SUVRp) images between 40 and 60 min post-injection of [^{11}C]BF-227 in an aged normal subject (64-year-old man), a sporadic CJD patient (CJD1, 63-year-old woman), a GSS patient (GSS2, 61-year-old man) and an AD patient (62-year-old woman). Compared to the aged normal subject and CJD patient, the GSS patient showed obvious [^{11}C]BF-227 retention in the cerebellum and temporal cortex. The AD patient also showed obvious [^{11}C]BF-227 retention in the temporal cortex; however, the cerebellum was relatively spared

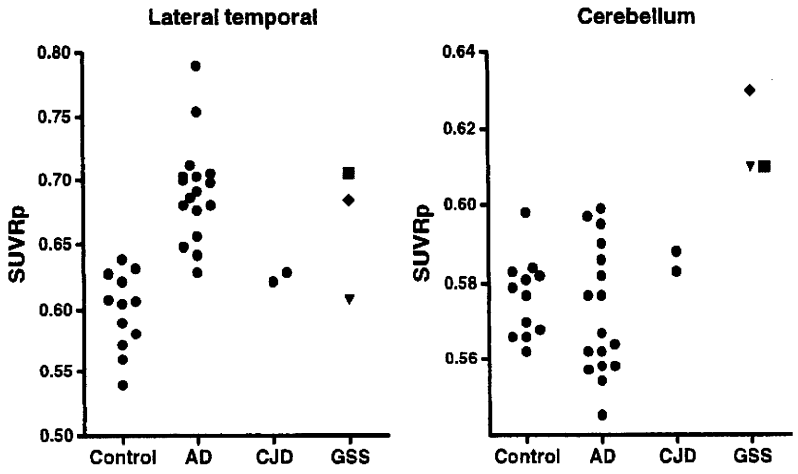

Fig. 4 SUVRp distribution in aged normal controls (*Control*), AD patients (*AD*), CJD patients (*CJD*) and GSS patients (*GSS*). GSS patients showed higher SUVRp values in the lateral temporal cortex and cerebellum. *Filled square* GSS1, *filled diamond* GSS2, *filled inverted triangle* GSS3

Discussion

This is the first study to demonstrate non-invasive detection of PrP amyloid plaques in GSS patients. GSS is neuropathologically characterized by deposits of multicentric amyloid plaques, which are especially abundant in the cerebellum, cerebral cortex and basal ganglia [3]. The present study demonstrated binding of BF-227 to PrP amyloid plaques in GSS brain sections. [^{11}C]BF-227 retention was observed in cortical and subcortical brain regions of GSS patients known for the high density of PrP plaques. Based on these findings, [^{11}C]BF-227 represents a promising candidate PET probe for the non-invasive detection of PrP amyloid plaques in the brain. However, the possibility that neocortical elevation of SUVRp in GSS patients might be caused by concomitant Aβ amyloid deposits or other misfolded protein deposits also should be considered, given that the two GSS patients showing prominent neocortical retention of [^{11}C]BF-227 were relatively older than the GSS patient showing no neocortical retention of BF-227. Although one positive GSS patient (GSS2) is still alive and was not examined neuropathologically, another positive case (GSS1) showed a high level of PrP amyloid deposits but no obvious deposits of Aβ amyloid or other misfolded proteins at autopsy. Furthermore, significant elevation of SUVRp was detected in the cerebellum, thalamus and hippocampus of all GSS cases. These brain regions are known to contain lower densities of Aβ plaques or other misfolded protein structures such as Lewy bodies. Based on these findings, it seems unlikely that concomitant deposition of Aβ amyloid or other misfolded proteins contributes to the high [^{11}C]BF-227 retention in GSS patients.

There is an increasing demand for in vivo detection of abnormal PrP deposition in the brain for the diagnosis of TSEs that might translate in early therapeutic intervention. Although GSS and other familial forms of TSEs can be diagnosed with PrP gene analysis using peripheral blood cells, it has been impossible to non-invasively measure the amount of abnormal PrP deposition in the brain. In a fashion similar to GSS, PrP amyloid deposition in the brain is commonly present in vCJD in which PrP amyloid plaques, called florid plaques, are pathognomonic [27]. Thus, [^{11}C]BF-227 PET might be a sensitive probe for the detection of PrP amyloid plaque deposition in vCJD as well as GSS, allowing longitudinal monitoring of PrP amyloid plaque deposition in the brain. Ante-mortem diagnosis of vCJD relies on the detection of abnormal PrP deposition in tonsil biopsy samples [28]. However, functional imaging using PET has an advantage over surgical biopsy tests in terms of both a non-invasive and an infection risk management point of view.

GSS is a rare form of TSE occurring in only about 3% of TSE cases in Japan. However, GSS is probably one of the TSEs most likely to benefit from early therapeutic interventions because the disease can be confirmed earlier using PrP gene analysis and progression occurs much more slowly than that in sporadic CJD, which comprises the majority of TSE cases. Recently, compounds such as pentosan polysulphate and doxycycline have been clinically used for experimental treatments for TSEs to prevent deposition of abnormal PrP in the brain, because these compounds slowed the disease progression in animal disease models when administered in an earlier stage of the disease [29–33]. Reliable surrogate markers are also required to evaluate the efficacy of these experimental interventions, and [^{11}C]BF-227 PET might be one of the best candidates to assess PrP amyloid deposition in GSS. However, it remains to be elucidated if PrP amyloid levels are a particularly relevant marker of therapeutic efficacy.

A previous PET study demonstrated moderate FDDNP retention and no remarkable PIB retention in the brain of two familial CJD patients with an octapeptide repeat insertion mutation [17]. A recent PET study has additionally demonstrated no PIB retention in two autopsy-confirmed sporadic

CJD patients [18]. In contrast with these studies, the present study successfully demonstrated prominent [^{11}C]BF-227 retention in the brain of GSS patients. Differences between the previous and present findings might mainly reside in the amount and type of PrP amyloid deposits in the brain, where histopathological studies indicate higher density of PrP amyloid plaques in GSS than in familial CJD [1]. In the present study, the findings in two sporadic CJD patients showing no obvious [^{11}C]BF-227 retention in the brain additionally support this speculation. The difference may also be attributable to higher binding affinity of BF-227 to PrP amyloid cores compared to FDDNP and PIB. To clarify this, further in vitro studies comparing the binding affinities of different amyloid tracers to PrP plaques in TSE brain homogenates are needed.

The youngest GSS patient (GSS3) showed BF-227 retention in the cerebellum and thalamus but not in the neocortex. The clinical symptoms in this patient were consistent with the brain distribution of BF-227, with the patient presenting with severe gait disturbance and slurred speech resulting from cerebellar ataxia but no signs of cognitive impairment, suggesting a close relationship between PrP plaque deposition as measured by BF-227 and regional brain dysfunction. There are variations of clinical phenotypes in GSS [1, 3]. Such variations are yet to be explained; however, the pattern of regional PrP amyloid distribution might be one of the factors affecting clinical phenotypes of GSS. In vivo PrP amyloid imaging using [^{11}C]BF-227 or other PET tracers will clarify neuropathological aspects of clinical variations in GSS.

In summary, we confirmed binding of BF-227 to PrP plaques in vitro and in vivo. A clinical PET study using [^{11}C]BF-227 demonstrated in vivo detection of PrP amyloid plaques in GSS patients. This imaging technique provides a potential means of facilitating both early diagnosis and non-invasive disease monitoring of certain forms of TSEs because, despite a lack of selectivity for PrP, brain retention of BF-227 in GSS shows a distinct pattern of regional distribution than that usually observed in sporadic AD.

Acknowledgment We appreciate the assistance of Dr. S. Watanuki, Dr. M. Miyake and Dr. H. Takashima in the clinical PET studies. This study was supported in part by the Program for the Promotion of Fundamental Studies in Health Science of the NIBIO in Japan, Industrial Technology Research Grant Program of the NEDO in Japan, and Health and Labor Sciences Research Grants (Translational Research and Research on Measures for Intractable Diseases) from the Ministry of Health, Labor, and Welfare of Japan.

References

1. DeArmond SJ, Kretzschmar HA, Prusiner SB. Prion diseases. In: Graham DI, Lantos PL, editors. Greenfield's neuropathology, 7th ed. London: Hodder Arnold. p. 273–323.
2. Collins SJ, Lawson VA, Masters CL. Transmissible spongiform encephalopathies. Lancet 2004;363:51–61.
3. Collins S, McLean CA, Masters CL. Gerstmann-Sträussler-Scheinker syndrome, fatal familial insomnia, and kuru: a review of these less common human transmissible spongiform encephalopathies. J Clin Neurosci 2001;8:387–97.
4. Noguchi-Shinohara M, Hamaguchi T, Kitamoto T, Sato T, Nakamura Y, Mizusawa H, et al. Clinical features and diagnosis of dura mater graft associated Creutzfeldt Jakob disease. Neurology 2007;69:360–7.
5. Lasmézas CI, Deslys JP, Demaimay R, Adjou KT, Hauw JJ, Dormont D. Strain specific and common pathogenic events in murine models of scrapie and bovine spongiform encephalopathy. J Gen Virol 1996;77(Pt 7):1601–9.
6. Schulz-Schaeffer WJ, Tschöke S, Kranefuss N, Dröse W, Hause-Reitner D, Giese A, et al. The paraffin-embedded tissue blot detects PrP(Sc) early in the incubation time in prion diseases. Am J Pathol 2000;156:51–6.
7. Fraser JR. What is the basis of transmissible spongiform encephalopathy induced neurodegeneration and can it be repaired? Neuropathol Appl Neurobiol 2002;28:1–11.
8. Small GW, Kepe V, Ercoli LM, Siddarth P, Bookheimer SY, Miller KJ, et al. PET of brain amyloid and tau in mild cognitive impairment. N Engl J Med 2006;355:2652–63.
9. Klunk WE, Engler H, Nordberg A, Wang Y, Blomqvist G, Holt DP, et al. Imaging brain amyloid in Alzheimer's disease with Pittsburgh Compound-B. Ann Neurol 2004;55:306–19.
10. Verhoeff NP, Wilson AA, Takeshita S, Trop L, Hussey D, Singh K, et al. In-vivo imaging of Alzheimer disease beta-amyloid with [11C]SB-13 PET. Am J Geriatr Psychiatry 2004;12:584–95.
11. Rowe CC, Ackerman U, Browne W, Mulligan R, Pike KL, O'Keefe G, et al. Imaging of amyloid beta in Alzheimer's disease with 18F-BAY94–9172, a novel PET tracer: proof of mechanism. Lancet Neurol 2008;7:129–35.
12. Kudo Y, Okamura N, Furumoto S, Tashiro M, Furukawa K, Maruyama M, et al. 2-(2-[2-Dimethylaminothiazol-5-yl]ethenyl)-6-(2-[fluoro]ethoxy)benzoxazole: a novel PET agent for in vivo detection of dense amyloid plaques in Alzheimer's disease patients. J Nucl Med 2007;48:553–61.
13. Ishikawa K, Doh-ura K, Kudo Y, Nishida N, Murakami-Kubo I, Ando Y, et al. Amyloid imaging probes are useful for detection of prion plaques and treatment of transmissible spongiform encephalopathies. J Gen Virol 2004;85:1785–90.
14. Bresjanac M, Smid LM, Vovko TD, Petric A, Barrio JR, Popovic M. Molecular-imaging probe 2-(1-[6-[(2-fluoroethyl)(methyl) amino]-2-naphthyl]ethylidene) malononitrile labels prion plaques in vitro. J Neurosci 2003;23:8029–33.
15. Sadowski M, Pankiewicz J, Scholtzova H, Tsai J, Li Y, Carp RI, et al. Targeting prion amyloid deposits in vivo. J Neuropathol Exp Neurol 2004;63:775–84.
16. Hoefert VB, Aiken JM, McKenzie D, Johnson CJ. Labeling of the scrapie-associated prion protein in vitro and in vivo. Neurosci Lett 2004;371:176–80.
17. Boxer AL, Rabinovici GD, Kepe V, Goldman J, Furst AJ, Huang SC, et al. Amyloid imaging in distinguishing atypical prion disease from Alzheimer disease. Neurology 2007;69:283–90.
18. Villemagne VL, McLean CA, Reardon K, Boyd A, Lewis V, Klug G, et al. 11C-PiB PET studies in typical sporadic Creutzfeldt-Jakob disease. J Neurol Neurosurg Psychiatry 2009;80:998–1001. doi:10.1136/jnnp.2008.171496.
19. Okamura N, Suemoto T, Shimadzu H, Suzuki M, Shiomitsu T, Akatsu H, et al. Styrylbenzoxazole derivatives for in vivo imaging of amyloid plaques in the brain. J Neurosci 2004;24:2535–41.
20. Ishikawa K, Kudo Y, Nishida N, Suemoto T, Sawada T, Iwaki T, et al. Styrylbenzoazole derivatives for imaging of prion plaques and treatment of transmissible spongiform encephalopathies. J Neurochem 2006;99:198–205.

21. Waragai M, Okamura N, Furukawa K, Tashiro M, Furumoto S, Funaki Y, et al. Comparison study of amyloid PET and voxel-based morphometry analysis in mild cognitive impairment and Alzheimer's disease. J Neurol Sci 2009;285:100–8. doi:10.1016/j.jns.2009.06.005.
22. Okamura N, Furumoto S, Funaki Y, Suemoto T, Kato M, Ishikawa Y, et al. Binding and safety profile of novel benzoxazole derivative for in vivo imaging of amyloid deposits in Alzheimer's disease. Geriatr Gerontol Int 2007;7:393–400.
23. Zeidler M, Gibbs CJ Jr, Meslin F. WHO manual for strengthening diagnosis and surveillance of Creutzfeldt-Jakob disease. Geneva: World Health Organization; 1998. p. 47–51.
24. McKhann G, Drachman D, Folstein M, Katzman R, Price D, Stadlan EM. Clinical diagnosis of Alzheimer's disease: report of the NINCDS-ADRDA Work Group under the auspices of Department of Health and Human Services Task Force on Alzheimer's Disease. Neurology 1984;34:939–44.
25. Friston KJ, Holmes AP, Worsley KJ, Poline JP, Frith CD, Frackowiack RSJ. Statistical parametric maps in functional imaging: a general linear approach. Hum Brain Mapp 1995;2:189–210.
26. Masters CL, Gajdusek DC, Gibbs CJ Jr. Creutzfeldt-Jakob disease virus isolations from the Gerstmann-Sträussler syndrome with an analysis of the various forms of amyloid plaque deposition in the virus-induced spongiform encephalopathies. Brain 1981;104:559–88.
27. Ironside JW, McCardle L, Horsburgh A, Lim Z, Head MW. Pathological diagnosis of variant Creutzfeldt-Jakob disease. APMIS 2002;110:79–87.
28. Hill AF, Zeidler M, Ironside J, Collinge J. Diagnosis of new variant Creutzfeldt-Jakob disease by tonsil biopsy. Lancet 1997;349:99–100.
29. Doh-ura K, Ishikawa K, Murakami-Kubo I, Sasaki K, Mohri S, Race R, et al. Treatment of transmissible spongiform encephalopathy by intraventricular drug infusion in animal models. J Virol 2004;78:4999–5006.
30. Rainov NG, Tsuboi Y, Krolak-Salmon P, Vighetto A, Doh-Ura K. Experimental treatments for human transmissible spongiform encephalopathies: is there a role for pentosan polysulfate? Expert Opin Biol Ther 2007;7:713–26.
31. De Luigi A, Colombo L, Diomede L, Capobianco R, Mangieri M, Miccolo C, et al. The efficacy of tetracyclines in peripheral and intracerebral prion infection. PLoS One 2008;3:e1888.
32. Teruya K, Kawagoe K, Kimura T, Chen CJ, Sakasegawa Y, Doh-ura K. Amyloidophilic compounds for prion diseases. Infect Disord Drug Targets 2009;9:15–22.
33. Forloni G, Salmona M, Marcon G, Tagliavini F. Tetracyclines and prion infectivity. Infect Disord Drug Targets 2009;9:23–30.

Original Research Article

Dementia and Geriatric Cognitive Disorders

Dement Geriatr Cogn Disord 2010;30:101–111
DOI: 10.1159/000318754

Accepted: June 15, 2010
Published online: August 21, 2010

Voxel-Based Analysis of Amyloid Positron Emission Tomography Probe [^{11}C]BF-227 Uptake in Mild Cognitive Impairment and Alzheimer's Disease

He Shao[a] Nobuyuki Okamura[a] Kentaro Sugi[a] Shozo Furumoto[a, b] Katsutoshi Furukawa[d] Manabu Tashiro[c] Ren Iwata[b] Hiroshi Matsuda[g] Yukitsuka Kudo[f] Hiroyuki Arai[d] Hiroshi Fukuda[e] Kazuhiko Yanai[a]

[a]Department of Pharmacology, Tohoku University Graduate School of Medicine, and Divisions of [b]Radiopharmaceutical Chemistry and [c]Cyclotron Nuclear Medicine, Cyclotron and Radioisotope Center, Tohoku University, and Departments of [d]Geriatrics and Gerontology, Division of Brain Sciences, and [e]Nuclear Medicine and Radiology, Institute of Development, Ageing and Cancer, Tohoku University, and [f]Innovation of New Biomedical Engineering Center, Tohoku University, Sendai, and [g]Department of Nuclear Medicine, Saitama Medical University, International Medical Center, Saitama, Japan

Key Words
Alzheimer's disease · Mild cognitive impairment · Positron emission tomography · Amyloid

Abstract
Aim: To determine early brain changes in the distribution of an amyloid positron emission tomography (PET) probe, ^{11}C-labeled BF-227 or [^{11}C]BF-227, in order to accurately predict the progression of mild cognitive impairment (MCI) to Alzheimer's disease (AD). ***Patients and Methods:*** Amyloid plaque burden was evaluated using [^{11}C]BF-227 PET in AD, MCI and aged normal controls. A voxel-based analysis of [^{11}C]BF-227 PET images was performed to characterize the culprit brain lesion in patients with MCI who were destined to progress to AD, referred to as MCI converters (MCI-C). In addition, binding characteristics of BF-227 to amyloid deposits were examined using postmortem AD brain samples. ***Results:*** Voxel-based statistical analyses of the BF-227 PET images clearly demonstrated an abnormal distribution of BF-227 mainly in the posterior association area in MCI-C and patients with AD. BF-227 uptake in the lateral temporal cortex was consistently observed in almost all MCI-C and patients with AD, and it distinguished MCI-C from MCI nonconverters. BF-227 binding strongly correlated with dense amyloid-β protein plaque density, but not with diffuse plaque density in the frontal cortex. ***Conclusion:*** BF-227 uptake in the lateral temporal cortex is a reliable indicator that can be used for predicting prognosis in patients with MCI.

Introduction

Alzheimer's disease (AD) is considered as the most common cause of dementia in the elderly. Since the extensive deposition of extracellular senile plaques is one of the pathological hallmarks of AD, many researchers have examined these lesions to try and understand the pathogenesis of AD. In 1984, amyloid-β protein (Aβ) was iso-

KARGER

Fax +41 61 306 12 34
E-Mail karger@karger.ch
www.karger.com

© 2010 S. Karger AG, Basel
1420–8008/10/0302–0101$26.00/0

Accessible online at:
www.karger.com/dem

Nobuyuki Okamura, MD, PhD
Department of Pharmacology, Tohoku University School of Medicine
2-1 Seiryo-machi, Aoba-ku
Sendai 980-8575 (Japan)
Tel. +81 22 717 8058, Fax +81 22 717 8060, E-Mail oka@mail.tains.tohoku.ac.jp

lated from cerebrovascular amyloidosis [1], and in the following year, it was isolated from amyloid plaques and neurofibrillary tangles [2, 3]. Senile plaques, which are mostly composed of Aβ, are believed to accumulate years before the onset of cognitive decline in AD [4]. Ten years ago, the concept of amnestic mild cognitive impairment (MCI) was introduced by the Mayo Clinic group. Amnestic MCI is now considered to be an intermediate predementia stage in patients with AD. Approximately 10–15% of patients with MCI develop AD [5, 6].

Positron emission tomography (PET) imaging using an amyloid-binding agent is a valid method for in vivo evaluation of Aβ plaque burden [7]. Several small molecular amyloid-binding agents have been designed for monitoring amyloid deposits in patients with MCI and AD and for evaluating the efficacy of antiamyloid therapy [8–12]. Furthermore, we have developed several benzoxazole derivatives as potential candidates for amyloid PET probes [13, 14]. A PET study using ^{11}C-labeled BF-227, or [^{11}C]BF-227, successfully detected amyloid plaques in living patients with AD [10]. Recent clinical studies have demonstrated neocortical [^{11}C]BF-227 uptake in patients with MCI [11, 15]. This finding suggests that neocortical [^{11}C]BF-227 uptake could be a potential biomarker for predicting progression from MCI to AD. In previous studies, analysis of PET images was mainly based on analysis of regions of interest (ROI). To eliminate any prior hypothesis about ROI selection, we performed voxel-based analyses of whole brain regions and made comparisons between MCI, AD and aged normal control groups. After [^{11}C]BF-227 PET scanning, we prospectively followed patients with MCI and investigated the relationship between initial BF-227 uptake and prognosis from MCI. The purpose of this study was to explore early changes in the process of amyloid plaque deposition in AD and understand the pattern of neocortical BF-227 distribution for accurate prediction of prognosis in the MCI stage.

Patients and Methods

Subjects and Patients

[^{11}C]BF-227 PET scans were performed on 12 aged normal controls, 19 probable patients with AD and 14 patients with MCI. The patients with AD were recruited via the Tohoku University Hospital Dementia Patients Registry, and the diagnosis was made according to the National Institute of Neurological and Communicative Diseases and Stroke/Alzheimer's Disease and Related Disorders Association criteria [16]. The patients with AD were divided into 2 groups according to their clinical severity: AD1 (Mini-Mental State Examination, MMSE, score ≥20) and AD2 (MMSE score <20). The diagnosis of amnestic MCI was made according to previously published criteria [5], which are as follows: (1) memory complaint, (2) normal activities of daily living, (3) normal general cognitive function, (4) abnormal memory for age, and (5) no sign of dementia. All patients with MCI underwent medical and neuropsychological reevaluation at approximately 3-month intervals and were divided into 2 groups: MCI converters (MCI-C; n = 7) and MCI nonconverters (MCI-NC; n = 7). MCI-C were defined as patients who eventually developed AD within a mean follow-up of 40.0 ± 6.9 months (range: 28–49 months), and MCI-NC were defined as patients having a transient memory loss or remaining cognitively stable for at least 3 years of follow-up (42.4 ± 2.2 months; range: 40–45 months). Aged volunteers who were taking no centrally active medication and who had no cognitive impairment or cerebrovascular lesion on MRI images were recruited as aged normal controls. All aged normal controls were screened via their medical history and responses to the MMSE. Subjects with medical conditions such as multiple cerebral infarctions, normal-pressure hydrocephalus, subdural hematoma, brain tumor, epilepsy, major depression, Parkinson's disease and other neurodegenerative diseases were excluded. In addition, asymptomatic cerebral infarction was not detected on T_2-weighted MRI images in the aged normal controls. The demographic data for all patients and aged normal controls are shown in table 1. The protocol of this study was approved by the Committee on Clinical Investigation at the Tohoku University School of Medicine, and by the Advisory Committee on Radioactive Substances at Tohoku University. Written informed consent was obtained from all patients and controls after complete description of the study. The clinical study was performed in accordance with the Declaration of Helsinki.

Radiosynthesis

BF-227 and its N-desmethylated derivative, a precursor to [^{11}C]BF-227, were synthesized by Tanabe R&D Service Co. (Osaka, Japan). [^{11}C]BF-227 was synthesized from the precursor by N-methylation in dimethyl sulfoxide, using [^{11}C]methyl triflate [10]. After quenching the reaction with 5% acetic acid in ethanol, [^{11}C]BF-227 was separated from the crude mixture by semipreparative, reversed-phase high-performance liquid chromatography and isolated from the collected fraction by solid-phase extraction. Purified [^{11}C]BF-227 was solubilized in isotonic saline containing 1% polysorbate 80 and 5% ascorbic acid. The saline solution was filter sterilized with a 0.22-μm Millipore filter (Millipore Co., Bedford, Mass., USA) for clinical use. At the end of synthesis, the radiochemical yields were greater than 50%, based on [^{11}C]methyl triflate, and the specific radioactivity ranged from 119 to 138 GBq/μmol. Radiochemical purities were greater than 95%.

Scanning Protocol

The [^{11}C]BF-227 PET study was performed using a SET-2400W PET scanner (Shimadzu, Kyoto, Japan). After intravenous injections of 211–366 MBq [^{11}C]BF-227, dynamic PET images were obtained for 60 min (23 sequential scans; 5 scans × 30 s, 5 scans × 60 s, 5 scans × 150 s, and 8 scans × 300 s) with closed eyes. All aged normal controls and patients underwent MRI using a 1.5-tesla MRI scanner (GE Signa Hispeed; GE Healthcare, Milwaukee, Wisc., USA). A 3-D volumetric acquisition of a T_1-weighted gradient echo sequence produced a gapless series of thin axial sections, using a vascular time-of-flight spoiled gradient echo sequence

Table 1. Demographic information on all the subjects

	Aged normal	MCI-NC	MCI-C	AD1	AD2	All AD
Number	12	7	7	10	9	19
Age, years	67.3 ± 2.7 (64–71)	77.6 ± 3.1* (74–82)	79.4 ± 4.2* (75–85)	72.9 ± 5.4 (65–85)	72.6 ± 7.3 (61–82)	72.7 ± 6.2 (61–85)
Gender (F/M), n	6/6	5/2	3/4	2/8	4/5	6/13
MMSE score	29.9 ± 0.3 (29–30)	26.3 ± 1.1 (25–28)	24.6 ± 3.4 (23–29)	22.7 ± 1.4* (21–25)	17.2 ± 2.9*,# (12–20)	20.1 ± 3.6 (12–25)
Years of education	13.2 ± 0.94	12.3 ± 0.48	11.9 ± 0.55	10.9 ± 0.72	10.3 ± 0.65	10.5 ± 0.42
GDS score	4.01 ± 0.44	4.32 ± 0.34	4.79 ± 0.31	4.23 ± 0.35	4.18 ± 0.46	4.20 ± 0.28

Values denote means ± SD with ranges in parentheses unless stated otherwise. Kruskal-Wallis test followed by Dunn's multiple comparison test. GDS = Geriatric Depression Scale. * $p < 0.05$ versus aged normal, # $p < 0.05$ versus MCI-NC.

(echo time/repetition time: 2.4/50 ms; flip angle: 45°; acquisition matrix: 256 × 256; 1 excitation; field of view: 22 cm; slice thickness: 2.0 mm).

Image Analysis

Standardized uptake value (SUV) images of [^{11}C]BF-227 were obtained by normalizing tissue concentration to injected dose and body weight. Average summations of SUV images were created from frames (20–40 min after injection) of dynamic PET images. Individual MR images were anatomically correlated with BF-227 PET images, using a statistical parametric mapping software (SPM5; Wellcome Department of Imaging Neuroscience, London, UK) [17]. ROI in the frontal cortex (Brodmann's areas, BA, 8, 9, 10, 44, 45, 46 and 47), lateral temporal cortex (BA 21, 22, 37 and 38), parietal cortex (BA 39 and 40), occipital cortex (BA 17), posterior cingulate cortex (BA 31) and cerebellar hemisphere were superimposed on MRI images, as described previously [10]. ROI information was then copied onto PET images, and regional SUV values at 20–40 min after injection were sampled using Dr. View/LINUX software (AJS, Tokyo, Japan). The cerebellum was used as the reference region. The regional-to-cerebellum SUV ratio (SUVR) was calculated and used as an index of BF-227 retention because the cerebellum is reported to be a region free of fibrillar amyloid plaques in the AD brain. Voxel-by-voxel comparisons between images from aged normal controls, patients with MCI and patients with AD were performed using SPM5 software. Spatial normalization was performed using an MR T_1 template of SPM5 to transfer PET images onto a standard stereotactic space. The normalized PET images were smoothed, using a 12 × 12 × 12 mm gaussian filter. The voxel count was normalized to the cerebellar ROI value. Images of the MCI-NC, MCI-C and AD groups, including patients with AD1 and AD2, were compared with those of the aged normal controls by means of a between-group analysis ($p < 0.05$ with false discovery rate correction; extent threshold: $k = 750$). For group analysis, a two-sample t test was used to detect differences among the groups.

In addition, a Z-score map of individual PET images was created for comparison between the mean and SD of the PET images of aged normal controls for each voxel. A software program named the Easy Z-Score Imaging System was used for this analysis [18]. Each PET SUV image was compared with the mean and SD of PET images of 15 aged normal controls (age: 58.9 ± 13.5 years; gender M/F: 10/5; MMSE score: 29.9 ± 0.2), using voxel-by-voxel Z-score analysis following voxel normalization to cerebellar ROI values according to the following formula: Z-score = (control mean – individual value)/control SD. Z-score maps were displayed by projection, with an averaged Z-score of 14 mm thickness to the surface rendering the anatomically standardized MRI template.

Neuropathological Staining

Postmortem brain tissue from an autopsy-confirmed AD case (87-year-old male) was obtained from the Tohoku University Hospital. Serial sections (6 μm thick) of paraffin-embedded blocks of temporal and frontal cortices were prepared in xylene and ethanol. Before staining, quenching of autofluorescence was performed by blanched sections in 0.25% potassium permanganate solution for 30 min. The sections were then treated with 0.1% potassium metabisulfite and 0.1% oxalic acid, followed by dipping briefly in water. The quenched tissue sections were immersed in 100 μmol/l of compound solution for 10 min and examined using a BX-51 fluorescence microscope (Olympus, Tokyo, Japan) equipped with a violet filter set (excitation: 380–420 nm; dichroic mirror: 430 nm; long-pass filter: 450 nm). Immunostaining was performed using monoclonal antibodies against Aβ (6F/3D; Dako, Glostrup, Denmark) at a dilution of 1:50. After pretreatment with formic acid for 5 min, the sections were placed in blocking solution for 30 min. After incubation with primary antibodies at 37°C for 60 min, the sections were processed by the avidin-biotin method using the Pathostain ABC-POD(M) kit (Wako) and chromogen DAB. The amyloid plaque morphology was classified into 2 types: (1) dense Aβ plaques including cored deposits with or without a ring of neuritic fibers, and (2) diffuse Aβ plaques including amorphous deposits. We randomly selected 20 areas (1.05 mm^2 per area) per section in the gray matter of the frontal and temporal cortices and counted the number of dense and diffuse Aβ plaques in each area. To estimate the capability of the compound to detect each kind of plaque, we examined the relationship between the number per unit area of positive staining using BF-227- and Aβ-specific antibody.

Statistical Analysis

Statistical comparisons of age among the 5 groups were performed using the Kruskal-Wallis test followed by Dunn's multiple comparison test. Statistical comparison of ROI results was performed via an analysis of variance followed by the Bonferroni method for multiple comparisons. Furthermore, effect size coefficients (Cohen's d) were calculated to evaluate group differences in PET measurements. The performance of diagnostic indices to

discriminate among groups was assessed using receiver operating characteristic (ROC) analysis. The area under the ROC curve (AUC) and SE were calculated and compared using GraphPad Prism software (GraphPad, San Diego, Calif., USA). Correlations between stainability of Aβ immunostaining and BF-227 staining were examined using the nonparametric Spearman rank correlation analysis. The paired t test was used to examine the difference in cored plaque density between the frontal and temporal cortices. Statistical significance for each analysis was defined as $p < 0.05$. These analyses were performed using GraphPad Prism software.

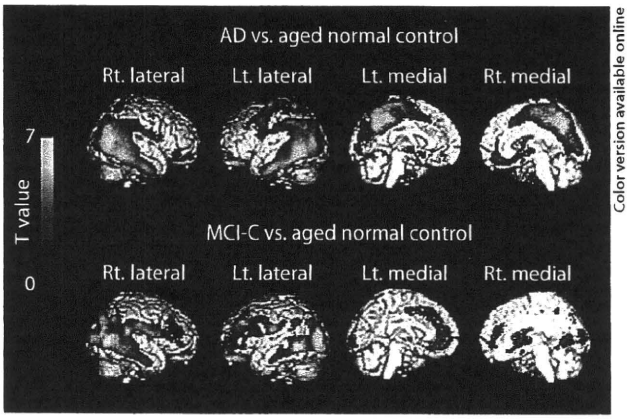

Fig. 1. Brain regions showing significantly higher uptake of [^{11}C] BF-227 in patients with AD (upper images) and MCI-C (lower images) compared with data from aged normal controls ($p < 0.05$, corrected for multiple comparisons). The red-to-yellow scale indicates the level of statistical significance of the differences in [^{11}C]BF-227 uptake (yellow: most significant difference).

Results

A statistically significant difference in age between aged normal controls and patients with MCI ($p < 0.05$) was observed. However, no statistically significant difference in age between MCI-C and MCI-NC as well as between aged normal controls and patients with AD was observed. Patients with AD showed a significantly lower MMSE score than aged normal controls. In addition, the AD2 group showed a significantly lower MMSE score than the MCI-NC group. However, no statistically significant difference in MMSE score was observed among other groups.

Voxel-based analysis of [^{11}C]BF-227 PET images demonstrated that MCI-C and patients with AD had significantly higher [^{11}C]BF-227 uptake in the neocortical region than aged normal controls (fig. 1; tables 2, 3). Bilateral temporoparietal BF-227 uptake was evident in both the AD and MCI-C groups although significant uptake in the posterior cingulate cortex and precuneus was observed only in the AD group. In the AD and MCI-C groups, the difference in the lateral frontal cortex was less evident compared with that in the lateral temporoparietal region. In contrast to the MCI-C group, the MCI-NC group showed no significant elevation of BF-227 uptake compared with the aged normal control group. Z-score maps of PET images were created by comparison with the normal control database (fig. 2). Most patients with AD showed a Z-score greater than 2 in the bilateral temporal and posterior cingulate cortices. In contrast, 10 out of the 12 aged normal controls (83%) showed no remarkable change in neocortical BF-227 uptake, except for 2 subjects (17%) showing modest changes in the lateral temporal and cingulate cortices. MCI-C tended to show higher neocortical Z-scores than MCI-NC (fig. 2b). Among the 7 MCI-C, 4 showed BF-227 uptake in the bilateral temporoparietal and frontal cortices, while the other 2 showed moderate abnormality in the temporal and frontal Z-scores. In MCI-C, changes in BF-227 uptake within the posterior cingulate cortex were relatively moderate compared with those in the lateral temporal cortex. One MCI-C showed limited change in BF-227 uptake within the temporal cortex and precuneus. In contrast to MCI-C, most MCI-NC showed no abnormal BF-227 uptake in the lateral temporal cortex, except for 1 who showed a slightly higher Z-score in the temporal cortex and an extremely high score in the posterior cingulate cortex. Another 3 MCI-NC also showed limited abnormality in the posterior cingulate cortex and precuneus but no abnormal Z-score in the lateral temporal cortex. No significant difference in BF-227 uptake was observed between the MCI-NC and MCI-C groups, MCI-NC and AD groups, and MCI-C and AD groups. Furthermore, no significant region showing reduction in BF-227 uptake in the MCI and AD groups compared with the aged normal controls was observed.

ROI analysis data were roughly consistent with voxel-based analysis data (fig. 3; table 4). The MCI-C group showed higher retention of [^{11}C]BF-227 in the frontal, temporal and parietal cortices than the aged normal control group. The AD1 group showed higher BF-227 retention in the frontal, temporal, parietal and occipital cortices than the aged normal control group. The AD2 group showed higher BF-227 retention in the temporal, parietal, occipital and posterior cingulate cortices than the aged normal control group, with the exception of the frontal cortex. Furthermore, significantly higher BF-227 uptake

Table 2. Talairach coordinates of within-cluster peak areas showing significantly higher BF-227 uptake in AD patients compared with aged normal group ($p < 0.05$, false discovery rate corrected)

k	T value	Talairach coordinates			Region
		x	y	z	
48,058	7.15 (5.38)	54	−46	−12	right inferior temporal gyrus
	6.79 (5.21)	50	−62	14	right middle temporal gyrus
	6.22 (4.92)	−52	−58	−2	left middle temporal gyrus
760	4.81 (4.09)	−24	4	−4	left putamen

Values in parentheses denote Z values.

Table 3. Talairach coordinates of within-cluster peak areas showing significantly higher BF-227 uptake in MCI-C compared with aged normal group ($p < 0.05$, false discovery rate corrected)

k	T value	Talairach coordinates			Region
		x	y	z	
14,893	6.19 (4.42)	46	−64	6	right middle temporal gyrus
	5.84 (4.27)	40	−74	14	right middle temporal gyrus
	5.52 (4.12)	52	−44	−8	right temporal lobe subgyrus
6,768	5.78 (4.24)	−36	32	34	left middle frontal gyrus
	4.78 (3.75)	−58	−16	24	left parietal lobe
	4.70 (3.71)	−24	50	0	left superior frontal gyrus
5,893	5.77 (4.24)	−38	−80	10	left middle occipital gyrus
	5.52 (4.12)	−42	−60	−4	left middle temporal gyrus
	5.27 (4.00)	−22	−92	−4	left cuneus

Values in parentheses denote Z values.

was found in the frontal and temporal cortices of the MCI-C group as well as in the temporal and parietal cortices of the AD group compared with the MCI-NC group. Compared with the AD group, Cohen's d was higher in the temporal (2.93) and parietal (2.25) cortices than in the frontal (1.69) and posterior cingulate (1.51) cortices for the aged normal control group. When comparing the MCI-C and MCI-NC groups, the highest Cohen's d was observed in the temporal (1.70) and parietal (1.76) cortices, followed by the frontal (1.62), posterior cingulate (0.85) and occipital (0.37) cortices, indicating that the difference in SUVR is the largest in the temporoparietal cortex when comparing the MCI-C and MCI-NC groups. Furthermore, ROC analysis demonstrated higher AUC values with the temporal SUVR (AUC = 0.987; SE = 0.016) than with the frontal SUVR (AUC = 0.915; SE = 0.052) for the discrimination between the AD and aged normal control groups as well as between the MCI-C and MCI-NC groups (fig. 4). Using the temporal BF-227 SUVR of 1.10 (1.5 SD above control mean) as the cutoff, a sensitivity of 95% and specificity of 92% in the discrimination between AD and aged normal groups, and a sensitivity of 100% and specificity of 57% in the discrimination between MCI-C and MCI-NC was achieved.

To explain why BF-227 preferentially accumulates in the temporal cortex as opposed to the frontal cortex of the AD brain, we examined the binding characteristics of BF-227 to Aβ deposits, using postmortem AD brain samples. BF-227 showed good stainability for dense-type plaques in the frontal and temporal cortices. Diffuse plaques in the frontal cortex tended to be larger than those in the temporal cortex. However, the stainability for diffuse-type plaques in the frontal cortex was relatively weaker than that in the temporal cortex (fig. 5). The mean number of Aβ plaques positively stained with BF-227 was significantly higher in the temporal cortex than in the fron-

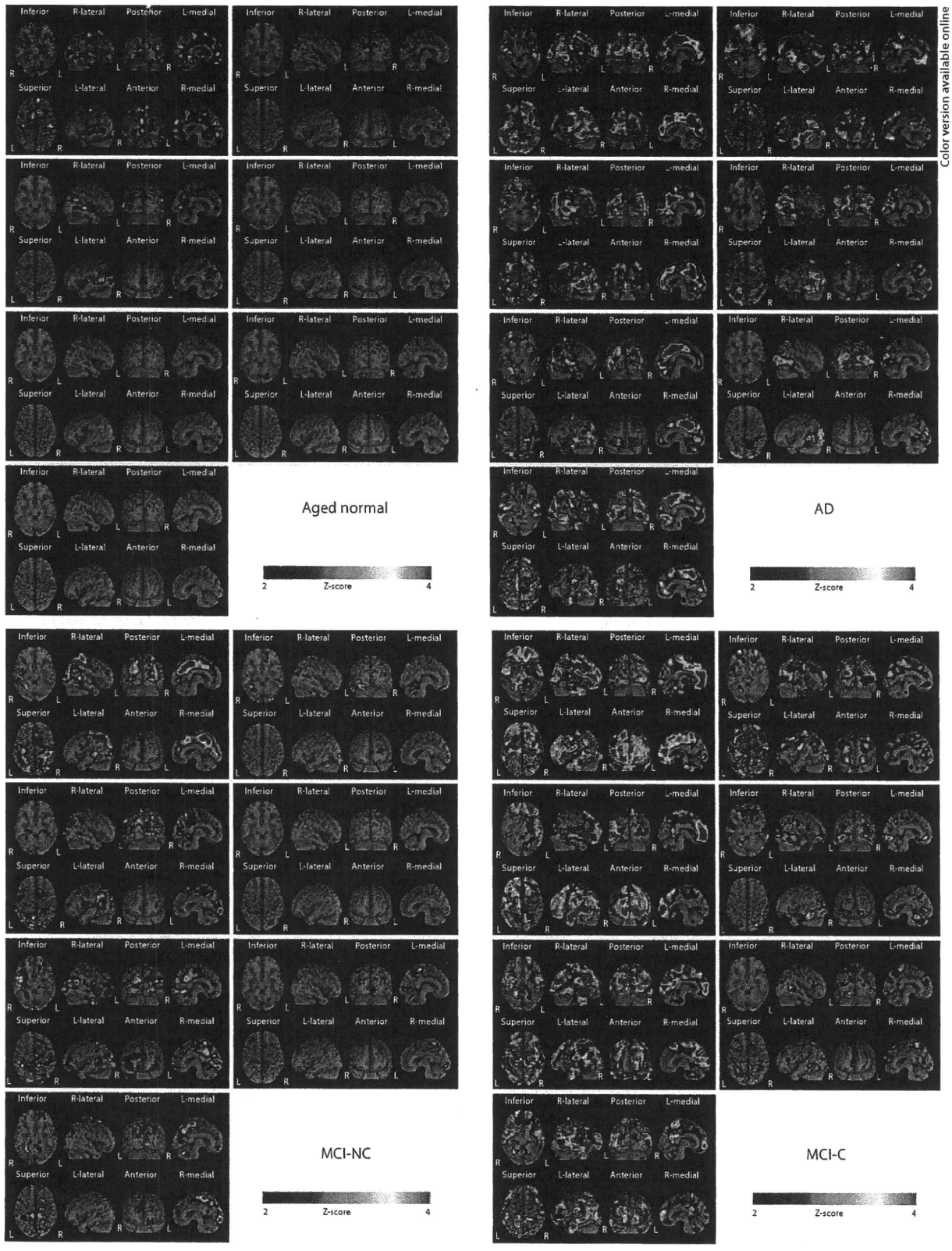
Color version available online
a
Inferior R-lateral Posterior L-medial
Superior L-lateral Anterior R-medial
Aged normal
AD
2 Z-score 4
b
MCI-NC
MCI-C

Table 4. Average SUVR between 20 and 40 min after injection

	SUVR					Cohen's d	
	aged normal	MCI-NC	MCI-C	AD1	AD2	MCI-NC and MCI-C	aged normal and all AD
Frontal	0.98 ± 0.05	0.98 ± 0.06	1.11 ± 0.10*,#	1.08 ± 0.08*	1.06 ± 0.05	1.62	1.69
Temporal	1.02 ± 0.04	1.06 ± 0.07	1.18 ± 0.07*,#	1.18 ± 0.07*,#	1.18 ± 0.06*,#	1.7	2.93
Parietal	1.06 ± 0.04	1.08 ± 0.05	1.17 ± 0.05*	1.18 ± 0.06*,#	1.19 ± 0.09*	1.76	2.25
Occipital	1.05 ± 0.04	1.09 ± 0.06	1.11 ± 0.06	1.13 ± 0.07*	1.13 ± 0.05*	0.37	1.51
Posterior cingulate	1.11 ± 0.07	1.12 ± 0.07	1.19 ± 0.10	1.20 ± 0.09	1.22 ± 0.05*	0.85	1.51

Values denote means ± SD. * $p < 0.05$ versus aged normal group; # $p < 0.05$ versus MCI-NC group.

tal cortex. In the temporal cortex, the number of positively stained Aβ plaques showed a significantly positive correlation with the number of dense- and diffuse-type plaques. However, in the frontal cortex, the number of positively stained Aβ plaques showed a significant correlation with only the number of dense-type plaques and not with the number of diffuse-type plaques (fig. 6).

Discussion

The identification of patients with a high risk of developing AD in the MCI stage is of great clinical value. However, it is difficult to predict the conversion from MCI to AD from a clinical and neuropsychological perspective. In comparison with MRI and CT, PET is relatively expensive and not accessible. Consequently, PET is not routinely used in the diagnosis of AD. However, PET imaging provides useful diagnostic information for predicting conversion from MCI to AD when MRI fails to provide sufficient information [15]. A recent Pittsburgh compound B (PiB) PET study demonstrated that in vivo detection of amyloid deposition provides useful prognostic information in MCI [19]. The present study using BF-227 PET showed similar predictive performance to previous PiB PET results although the signal-to-background ratio increase for BF-227 in patients with AD over controls was considerably lower than that for PiB. The lower signal-to-background ratio of BF-227 would be due to the lower detection sensitivity of BF-227 than that of PiB for diffuse plaques. However, BF-227 PET may have a better predictive value for progression from MCI to AD than PiB PET because the deposition of diffuse plaque is observed even during the normal aging process. A head-to-head comparison of BF-227 PET with PiB PET will clarify which tracer has more predictive power for conversion of MCI to AD.

Voxel-based analysis of PET images allows an objective and sensitive identification of regional change in uptake of the tracer. BF-227 is a PET tracer that binds to amyloid plaques in the brain [10]. Although BF-227 binds well to amyloid fibrils in vitro, the signal-to-background ratio for [^{11}C]BF-227 PET images was relatively lower than that for PiB PET, possibly due to the lower binding affinity of BF-227 to Aβ fibrils compared to PiB. This drawback can be overcome by voxel-based statistical comparison with a normal control database. In fact, the abnormal distribution of [^{11}C]BF-227 in MCI-C was more clearly demonstrated by Z-score mapping analysis than by unprocessed SUVR images. In addition, a portion of MCI-NC showed a high Z-score in the posterior neocortical areas, which may reflect early Aβ pathology in the brain. The pathological significance of these abnormalities will be elucidated after having followed up these patients.

A commonly observed feature in the Z-score maps of MCI-C and patients with AD was the change in bilateral temporal and temporooccipital cortices, which was also detected by between-group comparison with the aged

Fig. 2. a Voxel-by-voxel Z-score analysis of [^{11}C]BF-227 PET images for aged normal subjects (left) and patients with AD (right) with the mean and SD of PET images of 15 normal controls. The Z-score maps were displayed by the surface projection of the spatially normalized MR image. **b** Voxel-by-voxel Z-score analysis by comparison of [^{11}C]BF-227 PET images for MCI-NC (left) and MCI-C (right) with the mean and SD of PET images of 15 normal controls. The Z-score maps were displayed by the surface projection of the spatially normalized MR image.

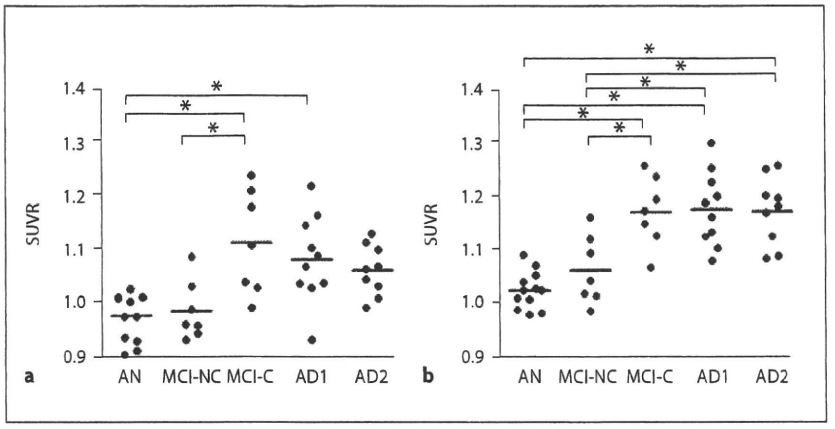

Fig. 3. Regional BF-227 SUVR in the frontal (**a**) and temporal (**b**) cortices. Horizontal bar: average SUVR in each group. * $p < 0.05$.

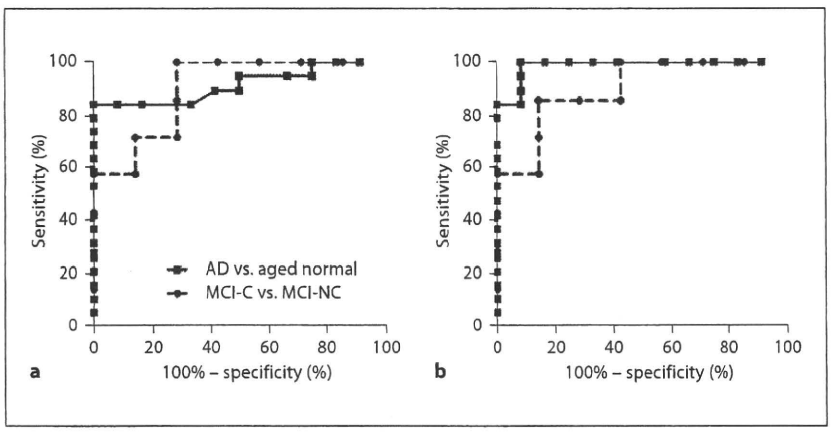

Fig. 4. ROC curves of regional BF-227 SUVR in the frontal (**a**) and temporal (**b**) cortices for differentiation between patients with AD and aged normal controls (solid line) and between MCI-C and MCI-NC (dashed line).

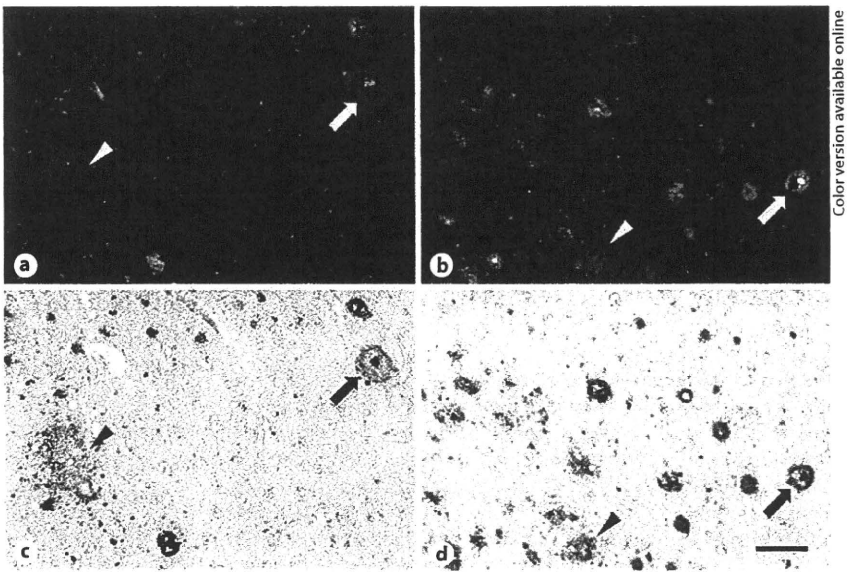

Fig. 5. Neuropathologic staining of AD frontal (**a**, **c**) and temporal (**b**, **d**) brain sections by BF-227. Cored plaques (arrows) are clearly stained with BF-227 (**a**, **b**). Cored-plaque staining with BF-227 correlates well with Aβ immunostaining in adjacent sections (**c**, **d**). Diffuse plaques (arrowheads) are faintly stained with BF-227 in the frontal brain section (**a**), but moderately stained in the temporal brain section (**b**). Scale bar = 100 μm.

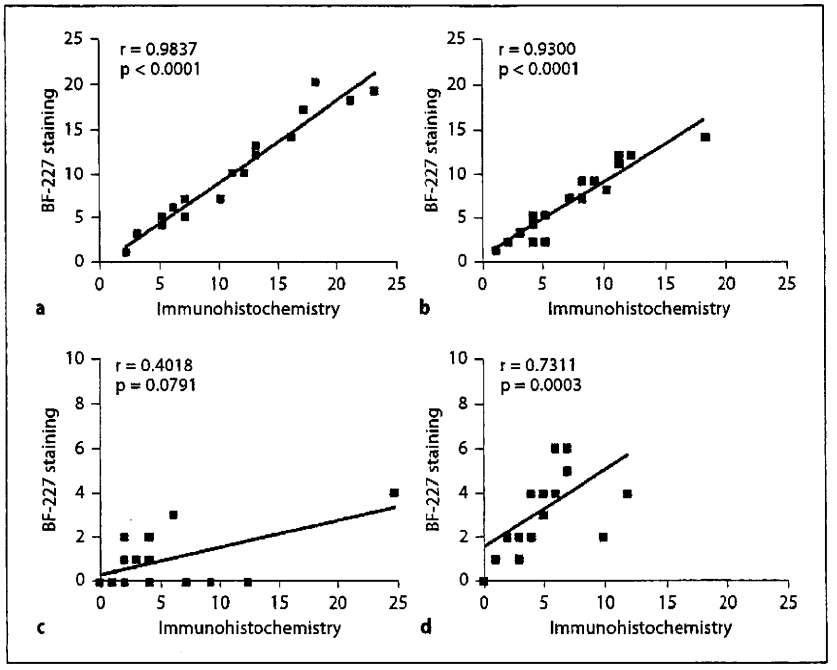

Fig. 6. Correlations between the numbers per unit area of amyloid plaques stained with Aβ-specific antibody and BF-227. The density of dense-type plaques showed a significant correlation with positive staining with BF-227 both in the frontal (**a**) and temporal (**b**) brain sections. However, the density of diffuse-type plaques was not correlated with BF-227 staining in the frontal cortex (**c**), and weakly correlated with BF-227 staining in the temporal cortex (**d**).

normal controls using the SPM software. The preferential [^{11}C]BF-227 retention in the posterior neocortical region corresponded with an area containing a high density of neuritic plaques [20]. This finding was confirmed by our analysis using postmortem AD brain samples. From these findings, the amount of dense plaque deposits in the posterior neocortical region, which could be measured by [^{11}C]BF-227 PET, is a reliable index of prognosis in patients with MCI. Interestingly, the Z-score mapping of BF-227 PET images further elucidated individual variation in the regional distribution of amyloid plaque deposition in patients with AD. There is great interest in determining the relationship between this heterogeneity and the clinical phenotype of patients with AD, which should be investigated in the future with data from a larger population. About 2/3 of patients with AD showed elevated BF-227 uptake in both anterior and posterior association areas, and the remaining 1/3 showed posterior-oriented BF-227 uptake. However, none of the patients with AD showed frontal-oriented BF-227 uptake. Although our analysis has been cross-sectional, these findings suggest that neuritic plaque deposition in AD starts at the posterior association areas and then spreads to other brain regions during AD progression.

The relatively lower [^{11}C]BF-227 retention in the frontal cortex of patients in the AD group may be a chance finding due to the small sample size. However, previous analysis of postmortem AD brain samples indicated that a majority of neocortical plaques start as fibrillar Aβ deposits and, in the late stages of AD, shift to nonfibrillar plaques [21]. Therefore, the relatively lower [^{11}C]BF-227 uptake in the AD group may be due to the transformation of fibrillar Aβ deposits to nonfibrillar Aβ deposits during AD progression. A longitudinal evaluation of [^{11}C]BF-227 uptake is necessary to examine whether the neocortical Aβ deposits reflected by BF-227 uptake change during the course of AD progression. In addition, the quantitative analysis of BF-227 binding to amyloid plaques should be performed in the future to eliminate the influence of regional cerebral hypoperfusion.

The definitive diagnosis of AD depends on postmortem examination because histological analysis of tissue samples is the only method for assessing AD pathology with certainty [7, 22]. Senile plaques were classified on the basis of the morphology of histopathological staining: diffuse plaques, primitive plaques, classical plaques and compacted plaques [23]. The diffuse plaques were abundant in healthy controls, whereas mature plaques such as primitive, classical and compact ones were typical in patients with AD. In our study, strong correlations between the number of mature plaques and BF-227 binding in the frontal and temporal cortices were observed. Further-

more, the temporal cortex exhibited a significant correlation between the number of diffuse-type plaques and BF-227 binding. However, the frontal cortex showed no such correlation. Generally, primitive, classical and compact plaques contain more amyloid fibrils than diffuse plaques. A previous electron microscopic examination has suggested that diffuse plaques in the frontal cortex contain a small amount of amyloid fibrils and do not easily transform to primitive plaques, while those in the temporal cortex contain more amyloid fibrils and tend to transform to primitive plaques [24]. Therefore, the binding ability of BF-227 to different types of diffuse plaques in the frontal and temporal cortices partly explains why BF-227 tends to accumulate in the temporal cortex of the AD brain. In addition, the density of dense-type plaques in the temporal cortex was higher than that in the frontal cortex in our analysis. This finding is in accordance with another comprehensive neuropathological examination that showed a higher density of amyloid plaques in the temporal cortex than in the frontal cortex [20, 25]. Thus, the lower density of primitive plaques in the frontal cortex may explain the relatively lower BF-227 uptake in the frontal cortex. Further analyses using more AD brain samples and radiolabeled BF-227 are required in the future because only one brain was examined in this study, and the concentration of BF-227 used to stain the postmortem tissue was not equivalent to the expected in vivo concentrations.

Previous PiB PET studies have shown the greatest tracer uptake in the precuneus and posterior cingulate cortex. However, our PET study demonstrated greater BF-227 uptake in the lateral temporal and parietal cortices of the AD brain samples than in the posterior cingulate cortex. A recent study demonstrated that the number of diffuse plaques in the posterior cingulate gyrus was greater than that in other neocortical areas. However, the number of neuritic plaques in the posterior cingulate cortex was not greater than that in other neocortical areas during AD progression [26]. Therefore, the modest posterior cingulate BF-227 uptake elevation in some patients with AD may be due to the lower binding affinity of BF-227 to diffuse plaques than that of PiB.

There are several limitations of this study. First, the sample size was small, primarily because of the limited follow-up period. Second, no repeat scans were performed to really assess changes in BF-227 uptake over time. Future studies should include longitudinal data from a larger sample. Third, the patients with MCI were older than the aged normal controls. Therefore, the higher neocortical uptake of [^{11}C]BF-227 in patients with MCI could be attributed to the effect of aging. However, no age-related change in BF-227 uptake was observed in the aged normal controls [10]. Furthermore, no significant elevation of [^{11}C]BF-227 uptake was observed in the MCI-NC group compared with that in the aged normal control group. Therefore, the higher [^{11}C]BF-227 uptake in the MCI-C group is not likely due to the effect of aging. We need to further address this issue by controlling for the age of normal controls and patients with MCI.

In summary, [^{11}C]BF-227 PET can detect the early Aβ load in the lateral temporal cortex of patients with MCI and AD. The amount of [^{11}C]BF-227 uptake in the temporal cortex was strongly related to prognosis in patients with MCI. BF-227 would be less subjective to amyloid pathology during the process of aging since this probe is believed to bind selectively to dense Aβ plaques. Thus, [^{11}C]BF-227 PET offers unique information concerning AD pathology that cannot be obtained by other PET tracers, which would be useful for the MCI population since it allows prediction of their risk for progression to AD in the near future.

Acknowledgments

This study was supported by the Health and Labor Sciences Research Grants for Translational Research from the Ministry of Health and the Grant-in-Aid for Scientific Research on Priority Areas – Integrative Brain Research from the Ministry of Education, Culture, Sports, Science, and Technology of Japan (20019006). We appreciate the technical assistance provided by Dr. S. Watanuki, Dr. Y. Ishikawa and M. Kato during the PET studies.

References

1 Glenner GG, Wong CW: Alzheimer's disease: initial report of the purification and characterization of a novel cerebrovascular amyloid protein. Biochem Biophys Res Commun 1984;120:885–890.

2 Masters CL, Multhaup G, Simms G, Pottgiesser J, Martins RN, Beyreuther K: Neuronal origin of a cerebral amyloid: neurofibrillary tangles of Alzheimer's disease contain the same protein as the amyloid of plaque core and blood vessels. EMBO J 1985;4:2757–2763.

3 Masters CL, Simms G, Weinman NA, Multhaup G, McDonald BL, Beyreuther K: Amyloid plaque core protein in Alzheimer disease and Down syndrome. Proc Natl Acad Sci USA 1985;82:4245–4249.

4 Hardy J, Selkoe DJ: The amyloid hypothesis of Alzheimer's disease: progress and problems on the road to therapeutics. Science 2002;297:353–356.